Computing 71, 175–204 (2003)
Digital Object Identifier (DOI) 10.1007/s00607-003-0027-1

Computing
Printed in Austria

# Adaptive Finite Element Methods for Microstructures? Numerical Experiments for a 2-Well Benchmark

**C. Carstensen,** Vienna, and **K. Jochimsen,** Kiel

Received December 5, 2002; revised June 5, 2003
Published online: September 25, 2003


**Abstract**

Macroscopic simulations of non-convex minimisation problems with enforced microstructures encounter oscillations on finest length scales – too fine to be fully resolved. The numerical analysis must rely on an essentially equivalent relaxed mathematical model. The paper addresses a prototype example, the scalar 2-well minimisation problem and its convexification and introduces a benchmark problem with a known (generalised) solution. For this benchmark, the stress error is studied empirically to asses the performance of adaptive finite element methods for the relaxed and the original minimisation problem. Despite the theoretical reliability-efficiency gap for the relaxed problem, numerical evidence supports that adaptive mesh-refining algorithms generate efficient triangulations and improve the experimental convergence rates optimally. Moreover, the averaging error estimators perform surprisingly accurate.

*Keywords:* adaptive finite element method, minimisation problem, convexification, relaxation, microstructures, a posteriori error estimate.

## 1 Introduction and Overview

Efficient macroscopic numerical simulations of non-convex minimisation problems rely on an essentially equivalent relaxed formulation [16, 17]. Based on Tartar's broken extremal example, this paper introduces a prototype example (1.2) and its relaxation (1.5). For this benchmark example, Theorem 2.1 below summarises the relations of infimising sequences of (1.2) and minimising sequences of (1.5) and gives closed formulae for the generalised solution $u$, the macroscopic stress field $\sigma$, and generated Young measure $\nu$ [3]. Since $u \notin W^{3/2,4}(\Omega)$ on the rectangle $\Omega := (0,1) \times (0,3/2)$ we have a counter example to higher regularity caused by the typical lack of smoothness at the interface between the region with microstructures and the region with a classical solution. This motivates the use of adaptive mesh-refining algorithms based on a posteriori error estimates. Since uniform control of gradient error norms is not accessible, those a posteriori error estimates suffer from the gap between efficiency and reliability: The efficient estimates are not reliable and the reliable estimates are not efficient. It is the aim of this paper to study the practical performance of the $P_1$ finite element method and its upper and lower error bounds for uniform and for adapted meshes empirically.

The model example has its origin is an anti-plane shear simplification of the Ericksen-James energy and serves as a master example for scalar non-convex energy densities. Given distinct $F_1$, $F_2$ in $\mathbb{R}^2$ for the non-convex 2-well energy density $W$, i.e.

$$W(F) := |F - F_1|^2 |F - F_2|^2 \quad \text{for } F \in \mathbb{R}^2, \tag{1.1}$$

we consider the non-convex energy functional

$$E(u) := \int_\Omega W(Du)dx + \int_\Omega |u - f|^2 dx. \tag{1.2}$$

The low-order term $|u - f|$ is motivated by a typical time-step discretization in time-depending problems.

The minimisation problem for (1.2) over all $u \in \mathscr{A} := u_0 + W_0^{1,4}(\Omega)$ on a rectangle $\Omega = (0,1) \times (0,3/2)$ is ill-posed and has, in general, no classical solution. The reason for non-attainment of a minimum is that high oscillations on finer and finer length-scales are necessary to lower the energy [4, 5, 9, 19, 27, 28]. Numerical simulations aim for the calculation of macroscopic properties of infimising sequences $(u_j)$ in $\mathscr{A}$. Examples are their weak limit $u \in \mathscr{A}$, interpreted as macroscopic displacement field, the macroscopic stress field $\sigma := DW^{**}(Du) \in L^{4/3}(\Omega; \mathbb{R}^2)$, and the Young measure $(\nu_x : x \in \Omega)$ which statistically describes oscillations of $(Du_j)$ in the limit $j \to \infty$ (see [3] and Theorem 2.1 below).

The non-convexity of $W$ may cause nightmares during the difficult computation of

$$u_h := \arg\ \min\{E(v_h) : v_h \in \mathscr{A}_h\} \quad \text{for } \mathscr{A}_h := u_{0,h} + \mathscr{S}_0^1(\mathscr{T}) \tag{1.3}$$

even if $u_h$ exists (uniquely) according to the finite dimension of the $P_1$ finite element space $\mathscr{S}_0^1(\mathscr{T})$. Since the (quasi-)convexification $W^{qc} = W^c = W^{**}$ is explicitly known, it is much more effective to calculate

$$u_h := \arg\ \min\{E^{**}(v_h) : v_h \in \mathscr{A}_h\} \tag{1.4}$$

for the relaxed energy functional

$$E^{**}(u) := \int_\Omega W^{**}(Du)dx + \int_\Omega |u - f|^2 dx. \tag{1.5}$$

The discrete relaxed solution $u_h$ from (1.4) does not show any oscillation and directly approximates the macroscopic displacement $u$. Based on the computed $u_h$, a simple post-processing yields approximations $\sigma_h$ to $\sigma$ and $\nu_h$ to $\nu$. Since $E^{**}$ is convex, standard software provides accurate solutions $u_h$ in very short CPU time.

The quasi-optimal convergence rate of the stress error $||\sigma - \sigma_h||_{L^{4/3}(\Omega)}$ is limited by the (lack of) regularity of an exact solution $u$. This paper studies an example with

a polynomial $f$ and a solution $u \in W^{3/2-\varepsilon,4}(\Omega)$ (for any $\varepsilon > 0$) based on Tartar's broken extremal in one dimension: There is no local higher regularity for non-convex minimisation problems.

In the benchmark example, we generally expect (reduced) convergence rates

$$\begin{aligned} ||u - Iu||_{L^2(\Omega)} &\propto h^{3/2}, \\ ||D(u - Iu)||_{L^4(\Omega)} &\propto h^{1/4}, \\ ||\sigma - \Pi\sigma||_{L^{4/3}(\Omega)} &\propto h \end{aligned}$$

in terms of the maximal mesh-size $h$ in a uniform triangulation (resp. a competing quality $h = 1/\sqrt{N}$ for a general 2D mesh with $N$ degrees of freedom); $I$ denotes nodal interpolation in $\mathscr{A}_h$ and $\Pi$ the $L^2$ projection onto $\mathscr{T}$-piecewise constants. The aim of this paper is to provide clear empirical evidence that the rigorous a priori and a posteriori analysis of [17], although based on quite sharp estimates, predict a numerical simulation too pessimistically. For instance, the quasi-optimal estimate

$$||\sigma - \sigma_h||_{L^{4/3}(\Omega)} \lesssim \inf_{v_h \in \mathscr{A}_h} ||D(u - v_h)||_{L^4(\Omega)} \leq ||D(u - Iu)||_{L^4(\Omega)} \tag{1.6}$$

predicts $||\sigma - \sigma_h||_{L^{4/3}(\Omega)} \propto h^{1/4}$, but we observe rather the much better convergence rate of $h^{3/4}$ in the numerical experiments of Section 5.

The convexified problem of this paper is generically not even strictly convex (i.e. $W^{**}$ is not strictly convex, see below). One resulting difficulty is that $||D(u - u_h)||_{L^4(\Omega)}$ is *not* controlled: The only rigorous error estimate reads $||D(u - u_h)||_{L^4(\Omega)} \lesssim 1$ while, and this came much as a surprise for us, we clearly observe

$$||D(u - u_h)||_{L^4(\Omega)} \propto h^{1/4} \tag{1.7}$$

in our numerical experiments below which, when compared with $||D(u - Iu)||_{L^4(\Omega)}$, appears optimal. In summary, numerical experiments suggests

$$\begin{aligned} ||u - u_h||_{L^2(\Omega)} &\propto h^{3/4}, \\ ||D(u - u_h)||_{L^4(\Omega)} &\propto h^{1/4}, \\ ||\sigma - \sigma_h||_{L^{4/3}(\Omega)} &\propto h^{3/4}. \end{aligned}$$

Adaptive mesh-refining algorithms are a well-established for improving the accuracy of approximations to non-smooth exact solutions of uniformly convex problems. At a certain point in the proof of related a posteriori error estimates for uniformly convex $W$, the error term $||D(u - u_h)||_{L^4(\Omega)}$ is absorbed. This is excluded in the benchmark for the not even strictly-convex relaxed energy $E^{**}$. The resulting difficulty leads to an efficiency-reliability gap in a posteriori error estimates. For instance, from [17],

$$||\sigma - \sigma_h||_{L^{4/3}(\Omega)} \lesssim \eta_R^{1/2} := \left( \sum_{T \in \mathscr{T}} \eta_T^R \right)^{3/8} \tag{1.8}$$

for the element-oriented residual refinement indicators

$$\eta_T^R = h_T^{4/3} \int_T |\mathrm{div}\sigma_h + f - u_h|^{4/3} dx + \int_{\partial T} h_E |J(\sigma_h \cdot n_{\mathscr{E}})|^{4/3} ds. \tag{1.9}$$

Here the second term counts jumps $J(\sigma_h \cdot n_{\mathscr{E}})$ of the discrete stress field $\sigma_h$ along interior edges $E \subset \partial T$ with normal vectors $n_E$. The estimator $\eta_R$ is reliable (i.e. an upper bound of the error, (1.8)) but *not* efficient. Indeed, from standard estimates [30] one can only expect (a local form of) the efficiency estimate (i.e., a lower bound of the error)

$$\eta_R \lesssim ||\sigma - \sigma_h||_{L^{4/3}(\Omega)} + \text{h.o.t.} \tag{1.10}$$

Notice carefully that we have $\eta_R$ in the power 1 in the efficiency estimate (1.10) and the power $1/2$ in the reliability estimate (1.8). This underlines our expectation that $\eta_R^\beta \propto ||\sigma - \sigma_h||_{L^{4/3}(\Omega)}$ for some $\beta$ with $1/2 \leq \beta \leq 1$. We observe the optimal $\beta = 1$ in our numerical experiments. We analyse two new error estimators,

$$\eta_Z := ||\sigma_h - A\sigma_h||_{L^{4/3}(\Omega)} \quad \text{and} \quad \eta_{D2} := \left( \sum_{T \in \mathscr{T}} \eta_{T,D2} \right)^{1/2} \tag{1.11}$$

where $A\sigma_h$ is an averaged stress field ($\mathrm{div}_{\mathscr{T}}$ denotes the piecewise divergence) and

$$\begin{aligned} \eta_{T,D2} := {} & ||h_T(\mathrm{div}_{\mathscr{T}}\sigma_h + 2(f - u_h))||_{L^{4/3}(T)} ||h_T D_h^2 u_h||_{L^4(T)} \\ & + h_E^{3/4} ||[\sigma_h \cdot n_E]||_{L^{4/3}(E)} ||h_T D_h^2 u_h||_{L^4(T_E)}. \end{aligned} \tag{1.12}$$

The ZZ-type error estimator $\eta_Z$ is motivated by recent success in the a posteriori analysis for uniformly convex problems [10, 11, 12, 18] where, up to higher order terms and multiplicative constants, $\eta_Z$ is reliable and efficient. Behind the estimator $\eta_{D2}$ is a (local) discrete analogue of $||D^2 u||_{L^4(\Omega)}$. This is an heuristic approach, but the resulting meshes and accuracies for all kind of (uniformly convex) problems perform well in goal-oriented error control and mesh-design applications [8]. Although we can merely provide the estimates

$$\eta_Z - \text{h.o.t.} \lesssim ||\sigma - \sigma_h||_{L^{4/3}(\Omega)} \lesssim \eta_Z^{1/2} + \text{h.o.t.}, \tag{1.13}$$

the striking numerical performance indicates that

$$||\sigma - \sigma_h||_{L^{4/3}(\Omega)} \approx \eta_Z \tag{1.14}$$

is an excellent error guess (as in [11, 13] for linear elliptic problems). The presented experimental results clearly support that $\eta_R^{1/2}$ and $\eta_Z^{1/2}$ are too pessimistic while $\eta_R$, $\eta_Z$, $\eta_{D2}$ correctly predict the empirical convergence rates; moreover, the averaging estimator $\eta_Z$ is exceptionally accurate. The final, possibly most important, issue is the practical performance of the three presented adaptive mesh-refining algorithms. We provide numerical evidence that the convergence rates for the stress error are optimally improved to

$$||\sigma - \sigma_h||_{L^{4/3}(\Omega)} \propto N^{-1/2} \approx h. \tag{1.15}$$

For the original non-convex problem with no theoretical foundation, the numerical results appear inconclusive and very depending on how the discrete non-convex global minimisation problem is approximately solved.

The remaining part of the paper is organised as follows. The mathematical models and the explicit (generalised) solution, with the link to the equivalent relaxed formulation, is surveyed in Section 2. Corresponding straightforward numerical models are introduced in Section 3 with numerical algorithms for the solution process and a comparison for uniformly refined meshes. A posteriori error estimates based on residuals, averaging, or approximation of curvature, are established in Section 4. Their efficiency-reliability gap is illustrated in Section 5 which also reports on numerical evidence for (1.8), (1.14)–(1.15).

## 2 Mathematical Model

Given the two distinct wells $F_1 := -(3,2)/\sqrt{13}$ and $F_2 := -F_1$, we consider the double well problem with the non-convex energy density from (1.1). Its lower convex envelope $W^{**}$ [16] is the convexified energy density (with $(\cdot)_+ := \max\{0, \cdot\}$)

$$W^{**}(F) = \Big((|F|^2 - 1)_+\Big)^2 + 4\Big(|F|^2 - ((3,2)\cdot F)^2/13\Big). \tag{2.1}$$

Let $\Omega = (0,1) \times (0,3/2)$. Set $t = (3(x-1) + 2y)/\sqrt{13}$ and define two functions $f$ and $g$ on $\Omega$ and $u_D$ on $\partial\Omega$ by

$$f(x,y) := f_0(t + 1/2) = -3t^5/128 - t^3/3, \tag{2.2}$$

$$g(x,y) := f_1(t + 1/2) = t^3/24 + t \tag{2.3}$$

$$\begin{aligned} u_D(0,y) &= \sqrt{13}(45657 - 92286y + 63144y^2 - 15472y^3 \\ &\quad + 720y^4 - 96y^5)/843648, \\ u_D(1,y) &= 2/\sqrt{13}y(4/13y^2 + 1), \\ u_D(x,0) &= -9\sqrt{13}(x-1)^3(81x^2 - 162x + 1745)/281216, \\ u_D(x,3/2) &= 3/\sqrt{13}x(x^2 9/13 + 1). \end{aligned} \tag{2.4}$$

Then, extend $u_D$ to a smooth function on $\mathbb{R}^2$ and let $\mathscr{A} := u_D + W_0^{1,4}(\Omega)$ be the set of all admissible deformations. The variational problem (P) reads

$$\text{(P)} \qquad \inf_{u\in\mathscr{A}} E(u) \quad \text{for} \quad E(u) := \int_\Omega \Big(W(\nabla u) + |u-f|^2\Big)dx.$$

The variational problem (24) reads

$$\text{(RP)} \qquad \min_{u\in\mathscr{A}} E^{**}(u) \quad \text{for} \quad E^{**}(u) := \int_\Omega \Big(W^{**}(\nabla u) + |u-f|^2\Big)dx.$$

**Theorem 2.1.** (*a*) *There exist infimising sequences of (P), i.e., there exists a sequence* $(u_j)$ *in* $\mathscr{A}$ *with*

$$\lim_{j\to\infty} E(u_j) = \inf E(\mathscr{A}) =: E_0.$$

(*b*) *The infimal energy equals* $E_0 = 0.10781476743659$.

(*c*) *Each infimising sequence* $(u_j)$ *in* (*P*) *is bounded and weakly convergent in* $W^{1,4}(\Omega)$. *The weak limit is unique and given by* (*recall* $t = (3(x-1)+2y)/\sqrt{13}$)

$$u(x,y) = \begin{cases} f_0(t+\frac{1}{2}) & \text{for } -\frac{1}{2} \le t \le 0, \\ f_1(t+\frac{1}{2}) & \text{for } 0 \le t \le \frac{1}{2}. \end{cases} \tag{2.5}$$

*The function u is displayed in Figure* 2. *The gradient of u reads*

$$Du(x,y) = \frac{1}{\sqrt{13}}\begin{pmatrix} 3 \\ 2 \end{pmatrix}\begin{cases} -\frac{15}{128}t^4 - t^2 & \text{for } -\frac{1}{2} \le t \le 0, \\ \frac{1}{8}t^2 + 1 & \text{for } 0 \le t \le \frac{1}{2}. \end{cases}$$

(*d*) *The infimal energy* $E_0$ *is not attained in* (*P*), *i.e.*,

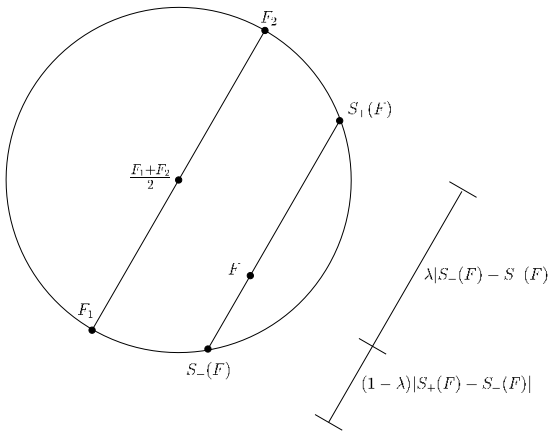


**Fig. 1.** Geometric interpretation of the support $S_\pm(F)$ and the convex coefficient $\lambda(x)$ of $v_x(F) = \lambda(F)S_+(F) + (1-\lambda(F))S_-(F)$

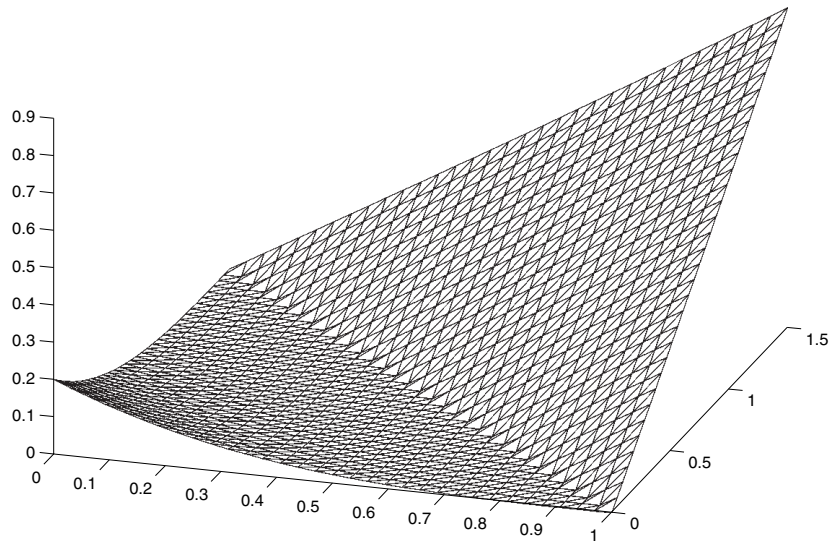


**Fig. 2.** Nodal interpolation $I\,u$ of exact (generalised) solution $u$ from (2.5) on a uniform $32 \times 32$ grid with 2048 elements

$$E_0 < E(v) \quad \textit{for all } v \in \mathscr{A}.$$

(*e*) *The problem* (*RP*) *has a unique solution u given by* (2.5). *It is characterised as the solution of the Euler-Lagrange equation*

$$\int_\Omega \sigma \cdot Dv\,dx + 2\int_\Omega (u-f)\,v\,dx = 0 \quad \textit{for all } v \in W_0^{1,4}(\Omega), \tag{2.6}$$

*where*

$$\sigma := DW^{**}(Du) = (3,2)/\sqrt{13}\begin{cases} 0 & \textit{for } -1/2 \le t \le 0, \\ t^2(1+3t^2/16+t^4/64) & \textit{for } 0 \le t \le 1/2. \end{cases} \tag{2.7}$$

(*f*) *There holds*

$$E_0 = E^{**}(u) = \min E^{**}(\mathscr{A}) < E^{**}(v) \quad \textit{for all } v \in \mathscr{A} \setminus \{u\}.$$

(*g*) *Any infimising sequence* $(u_j)$ *of* (*P*) *is bounded in* $W^{1,4}(\Omega)$ *and generates a Young measure* $(\nu_x)$, *i.e. there exists a family* $(\nu_x)_{x\in\Omega}$ *of probability measures* $\nu_x$ *which satisfies*: *Given any measurable* $\omega \subset \Omega$ *and any* $f \in C_0(\Omega)$ (*i.e.* $f : \Omega \to \mathbb{R}$ *is continuous and* $\lim_{|x|\to\infty} f(x) = 0$), *there holds*

$$\lim_{j\to\infty} \int_\omega f(Du_j)dx = \int_\omega \langle \nu_x, f\rangle\,dx.$$

*The Young measure is unique and reads*

$$\nu_x := \lambda(Du(x))\delta_{S_+(Du(x))} + (1 - \lambda(Du(x)))\delta_{S_-(Du(x))}, \tag{2.8}$$

*where* $F = Du$, $P := I - F_2 \otimes F_2$, *and*

$$\begin{aligned} \lambda(F) &:= \frac{1}{2}(1 + F_2^T \cdot F(1 - |P \cdot F|^2)^{-1/2}) \in [0,1], \\ S_\pm(F) &:= \begin{cases} P \cdot F \pm F_2(1 - |P \cdot F|^2)^{-1/2} & \text{for } |F| < 1, \\ F & \text{for } 1 < |F|. \end{cases} \end{aligned} \tag{2.9}$$

*See Figure* 1 *for an illustration of* $S_\pm(F)$ *and Figure* 3 *for a plot of the volume fraction* $\lambda(Du)$.

(*h*) *Any infimising sequence* $(u_j)$ *of* (*P*) *generates a sequence of stresses* $(\sigma_j)$ *by* $\sigma_j := DW\ (Du_j)$ *which is convergent in measure towards* $\sigma$ *from* (2.7).

*Proof.* Parts of the assertions are properly-stated particular cases of more general results in relaxation theory [2, 6, 9, 10, 16, 19, 22, 27, 28]. The necessary growth and smoothness assumptions are directly verified for the example at hand. The necessary detailed calculations start with the proof of (2.6) for $u, f$ and $\sigma$ given in

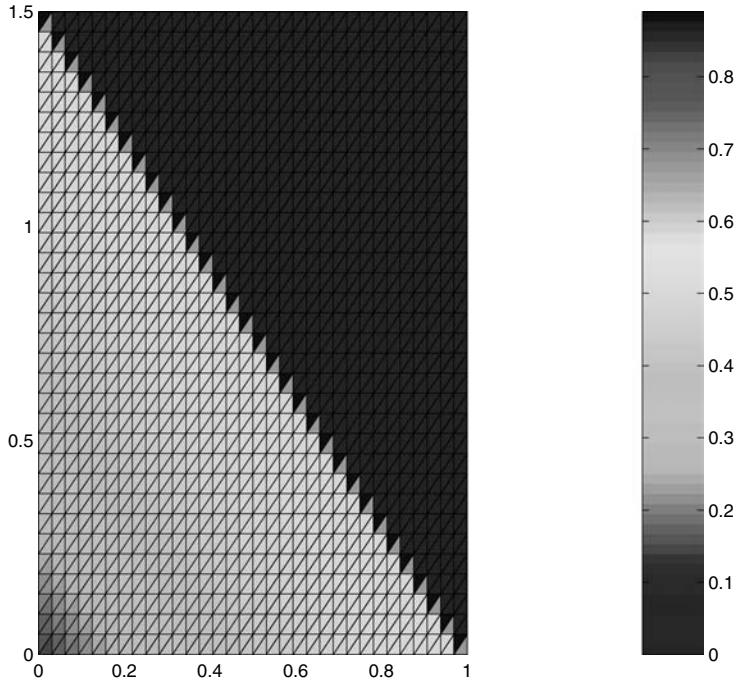


**Fig. 3.** Volume fractions $\lambda$ computed with (2.9) for $F = DIu$ and the nodal interpolation $Iu$ of the exact solution $u$ from Figure 2

(2.5), (2.2), and (2.7), respectively. The derivative $Du$ of $u$ is directly established and so is

$$\operatorname{div} \sigma = 2(u - f) \quad \text{in } \mathscr{R} := \operatorname{conv}\{(1,0),(1,3/2),(0,3/2)\}$$

while $\sigma = 0$ and $u = f$ in the remaining part $\mathscr{M} := \operatorname{con}\{(0,0),(1,0),(0,3/2)\}$. Note that $J(\sigma \cdot n) = 0$ along the antidiagonal $\mathscr{M} \cap \mathscr{R}$. This and an integration by parts verify (2.6). It follows from the quadratic lower-order term that the solution is unique [16]. Therefore, any infimising sequence (not just a subsequence) converges weakly towards $u$. This proves (a) and (c), while (b) results from a direct integration of $W^{**}(Du)$ in $\mathscr{R}$ ($W^{**}(Du) = 0$ in $\mathscr{M}$). The assertions (d), (e), and (f) follow from general relaxation theorems and (2.6) combined with the uniqueness of a solution $u$. The assertion (g) is a particular version of the fundamental theorem of Young measures [2, 19, 27, 28]; Formula (2.9) is known from [16]. The assertion (h) can be deduced from [23]. □

**Remark 2.1 (More general situation).** The presented formulae are special cases of a 2-well problem in [16] with general wells $F_1$ and $F_2$. Therein, one finds general expressions for the related relaxed energy density (1.1) or the formula (2.9) to recover the Young measure. The description here focuses on a benchmark situation under minimal notation with an explicit solution $u$ based on Tartar's one-dimensional broken extremal [26, 29].

**Remark 2.2 (Counterexample for higher regularity).** The only regularity result on the gradients known to us is due to Chipot & Evans [21]. Under quadratic growth conditions, the minimiser in (RP) is Lipschitz continuous. Here, quadratic growth is not important (as $\|\nabla u\|_\infty$ is bounded) and $u$ is even globally Lipschitz continuous. The generalised solution is depicted in Figure 2 through a plot of the nodal interpolant $Iu$ with respect to a uniform mesh. Higher regularity does not hold although the function $f$ is smooth and $\Omega$ is convex. Hence, $u$ is a counterexample to $H^2$ regularity for degenerately convex minimisation problems.

**Remark 2.3 (Stress regularity).** Owing to [15], $\sigma \in W^{1,2}_{loc}(\Omega)$ and, here, $\sigma \in W^{1,2}(\Omega)$ holds even globally.

**Remark 2.4 (Microstructure domain).** The lower left triangle $\mathscr{M} := \operatorname{conv}\{(0,0)\}$, $\{(1,0)\}$, $\{(0,3/2)\}$ is the microstructure domain with a nontrivial Young measure $\nu_x$. In the remaining regular part $\mathscr{R} := \operatorname{conv}\{(1,0),\ (3/2,1),(0,3/2)\}$, the Young measure is trivial (a Dirac measure almost everywhere). The interpretation is that we expect finer and finer oscillations in $\mathscr{M}$ with gradients that oscillate between two phases $S_+$ and $S_-$. The volume fraction $\lambda$ gives the probability for $S_+$ and $(1-\lambda)$ the probability for $S_-$; the volume fraction $\lambda$ is computed for $F = DIu$ ($Iu$ from Figure 2) via (2.9) and displayed in Figure 3.

## 3 Numerical Model

The Galerkin discretization with a discrete space $\mathscr{S}^1_0(\mathscr{T})$ is based on a regular triangulation $\mathscr{T}$ into triangles; i.e., $\mathscr{T}$ is a set of closed triangles and two distinct triangles $T_1$ and $T_2$ satisfy that $T_1 \cap T_2$ is either empty, a single vertex $z$, $T_1 \cap T_2 = \{z\}$, or a common edge $E$, $T_1 \cap T_2 = E$. The set of all edges and vertices (also called nodes) is $\mathscr{E}$ and $\mathscr{N}$, respectively. Then,

$$\mathscr{S}^1(\mathscr{T}) := \{v_h \in C(\bar{\Omega}) : \forall T \in \mathscr{T}, v_h|_T \text{ is affine}\}, \tag{3.1}$$

$$\mathscr{S}^1_0(\mathscr{T}) := \{v_h \in \mathscr{S}^1(\mathscr{T}) : v_h = 0 \text{ on } \partial\Omega\}. \tag{3.2}$$

Let $\mathscr{K} := \mathscr{N} \cap \Omega$ denote the set of free nodes and $(\varphi_z : z \in \mathscr{K})$ be the nodal basis of $\mathscr{S}^1_0(\mathscr{T})$; $\varphi_z$ is the hat function of the node $z \in \mathscr{K}$, i.e., $\varphi_z \in \mathscr{S}^1(\mathscr{T})$ with $\varphi_z(z) = 1$ and $\varphi_z(x) = 0$ for all $x \in \mathscr{N} \setminus \{z\}$. The Dirichlet conditions $u_D$ are discretised by nodal interpolation, i.e., $u_{D,h} \in \mathscr{S}^1(\mathscr{T})$ with

$$u_{D,h} = u_D(z) \quad \text{if } z \in \mathscr{K} \quad \text{and} \quad u_{D,h} = 0 \quad \text{if } z \in \mathscr{N} \setminus \mathscr{K}, \tag{3.3}$$

and $\mathscr{A}_h := u_{D,h} + \mathscr{S}^1_0(\mathscr{T})$ replaces $\mathscr{A}$ in (RP). The resulting discrete problem ($\mathrm{RP}_h$) reads

$$(\mathrm{RP}_h) \qquad \min_{u_h \in \mathscr{A}_h} E^{**}(u_h).$$

**Theorem 3.1.** (*a*) *There exists a unique solution $u_h$ of ($RP_h$); the functional $E^{**}$ is uniformly convex on $\mathscr{A}_h$.*

(*b*) *The discrete solution $u_h$ is characterised by the discrete Euler-Lagrange equations*

$$\int_\Omega DW^{**}(Du_h) \cdot \nabla\varphi_z \, dx + 2\int_\Omega (u_h - f)\varphi_z \, dx = 0 \quad \textit{for all } z \in \mathscr{K}. \tag{3.4}$$

(*c*) *Let $u$ denote the (generalised) solution of (P) defined in Theorem* 2.1 *and abbreviate $\sigma = DW^{**}(Du)$ and $\sigma_h := DW^{**}(Du_h)$. Then,*

$$||\sigma - \sigma_h||_{L^{4/3}(\Omega)} + ||u - u_h||_{L^2(\Omega)} \le C|u - Iu|_{W^{1,4}(\Omega)}$$

*with a mesh-independent constant $C$.*

*Proof.* Since the affine space $\mathscr{A}_h$ is of finite dimension, the uniform convexity of the $L^2$ contribution $||u_h - f||^2_{L^2(\Omega)}$ yields a uniform convex energy functional $E^{**} : \mathscr{A}_h \to \mathbb{R}$, i.e.,

$$||v_h - w_h||^2_{L^2(\Omega)} \le DE^{**}(v_h, v_h - w_h) - DE^{**}(w_h, v_h - w_h) \quad \text{for all } v_h, w_h \in \mathscr{A}_h.$$

Although the $L^2$ norm is weaker then the $W^{1,4}$ norm, this estimate and obvious growth conditions prove (a) for a fixed discrete space $\mathscr{A}_h$.

Owing to uniform convexity, each stationary point is a global minimiser. The identity (b) then follows from a straightforward derivation. The a priori error estimate (c) is verified in [16]. □

**Remarks 3.1.** (a) The numerical solution of (3.4) is performed with a simple Newton-Raphson scheme which reads: Given $x^{(v)} \in \mathbb{R}^n$, find $x^{(v+1)} \in \mathbb{R}^n$ with $u_h^{(v+1)} := \sum_{y\in\mathscr{K}} x_y^{(v+1)}\varphi_y$ such that

$$A^{(v)}(x^{(v+1)} - x^{(v)}) = b^{(v)}. \tag{3.5}$$

Here, $(x_y^{(v)} : y \in \mathscr{K})$ denotes the coefficient vector, $n := \operatorname{card}\mathscr{K} = \dim \mathscr{A}_h$, and, for any $y, z \in \mathscr{K}$,

$$A_{yz}^{(v)} := \int_\Omega D^2W^{**}(Du_h^{(v)})D\varphi_y D\varphi_z\,dx + 2\int_\Omega \varphi_y\varphi_z\,dx, \tag{3.6}$$

$$b_y^{(v)} := \int_\Omega DW^{**}(Du_h^{(v)})D\varphi_y\,dx + 2\int_\Omega (u_h^{(v)} - f)\varphi_y\,dx. \tag{3.7}$$

(b) The implementation of (3.5) in the spirit of [1] directly solves the sparse linear system of equations (3.5). Therein, for $G, H \in \mathbb{R}^2$ and the Heavyside function $\mathbb{H} : \mathbb{R} \to \{0, 1\}$, $\mathbb{H}(x) = 0$ for $x \le 0$ and $\mathbb{H}(x) = 1$ for $x > 0$,

$$\begin{aligned} DW^{**}(F)(G) &= 4\Big(|F|^2 - 1\Big)_+ F\cdot G + 8(F\cdot G - (F_2\cdot F)(F_2\cdot G)),\\ D^2W^{**}(F)(G)(H) &= \Big(4\Big(|F|^2-1\Big)_+ + 8\Big)(H\cdot G)\\ &\quad + 8\mathbb{H}\Big(|F|^2-1\Big)(F\cdot G)(F\cdot H) - 8(F_2\cdot H)(F_2\cdot G). \end{aligned}$$

(c) In our numerical examples repeated below, the initial vector $x^{(0)}$ was chosen by zero; hence $u_{D,h}$ from (3.3) was the initial displacement. Then a few numbers by of iterations are necessary to compute an accurate coefficient vector.

(d) Throughout the error analysis in [16] the fact $\mathscr{A}_h \not\subset \mathscr{A}$ according to the interpolation error $u_{D,h} \neq u_D$ on $\partial\Omega$ was ignored. This error is of higher order and hence of minor influence in the analysis. The a priori estimates of Theorem 3.1, however, are *not* affected.

The numerical result of a Newton-Raphson scheme is displayed in Figure 4 and 7. The underlying uniform mesh is the same as in Figure 2. At first glance the results are comparable, but a closer look shows that the antidiagonal interface $\mathscr{M} \cap \mathscr{R}$ leads to a sharp edge in $u$ but not in the deformed mesh from $u_h$. The discrete approximation $u_h$ appears too smooth and develops no sharp interface. Generically, the mesh $\mathscr{T}$ cannot resolve the interface $\Gamma = \mathscr{M} \cap \mathscr{R}$ between the region with and without microstructure. Here, the geometry $\Omega = (0, 1) \times (0, 3/2)$ is chosen such that any uniform mesh (based on a grid aligned to $\Omega$) does not resolve

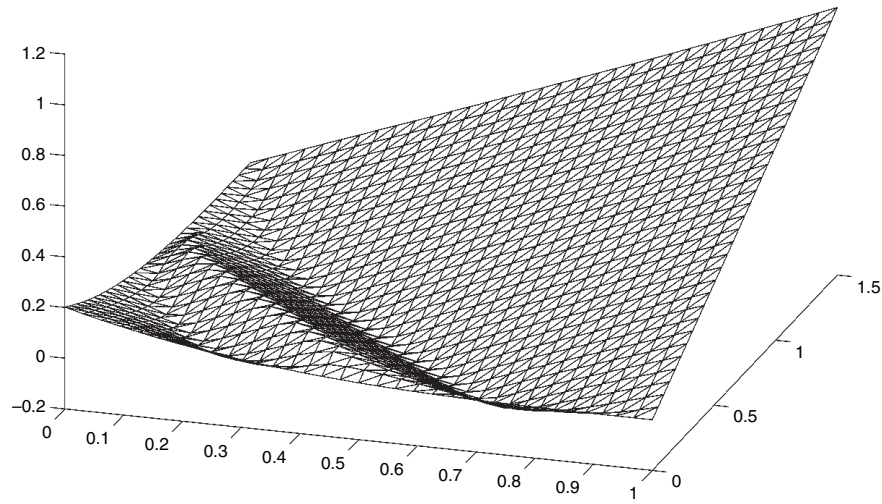


**Fig. 4.** Deformation of $\Omega$ in problem $(P_h)$ on a uniform $32 \times 32$ grid with 2048 elements

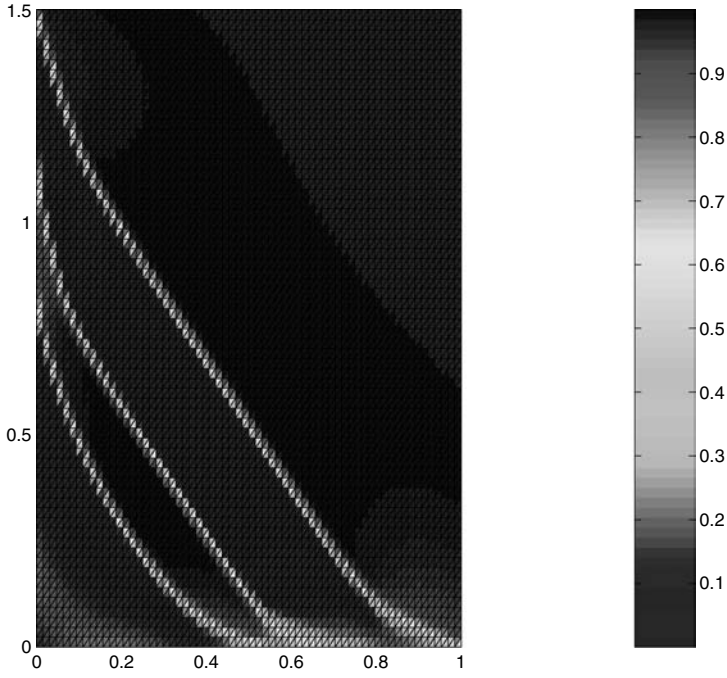


**Fig. 5.** Volume Fractions in problem $(P_h)$ on a uniform grid based on the deformation from Figure 4

the antidiagonal $\Gamma = \mathscr{M} \cap \mathscr{R}$. As a consequence, the generalised solution $u$ is not well resolved near $\Gamma$.

For comparison, we aimed to calculate an approximate minimiser of $(P_h)$,

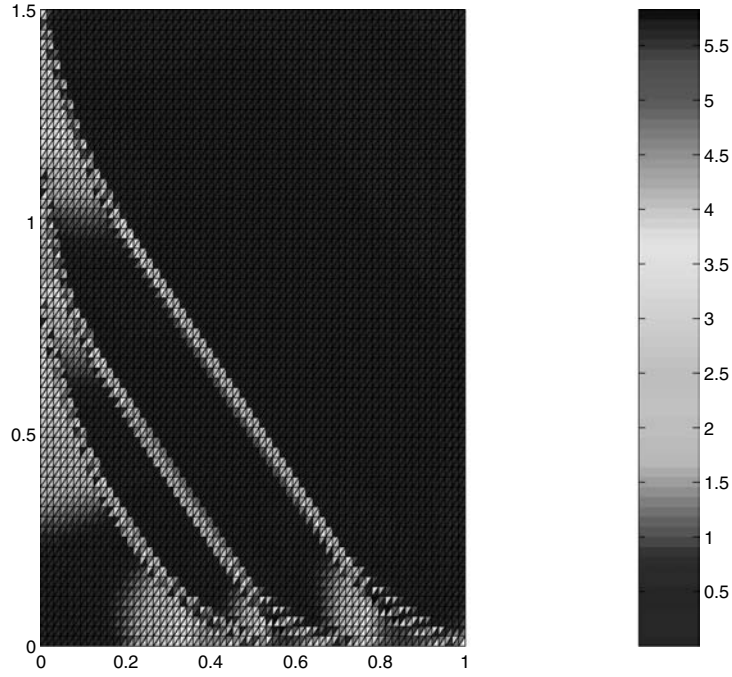


**Fig. 6.** Tension $|\sigma_h|$ in $\Omega$ in problem $(\mathrm{P}_h)$ on a uniform $32 \times 32$ grid with 2048 elements

$$(\mathrm{P}_h) \qquad \min_{u_h \in \mathscr{A}_h} E(u_h),$$

with respect to the same mesh $\mathscr{T}$. After 416 iterations of Newton-Raphson's method we obtained the approximation displayed in Figure 4. In this picture we observe oscillations, at least, on a very coarse scale, we see a bubble in $\mathscr{M}$ which might be the 2D analogue of a sea-saw microstructure. Beside this bubble, the overall picture looks similar to the generalised and relaxed discrete solution $Iu$ and $u_h$ of Figure 2 and 4, respectively. From Figure 2 and 4 it is hard to say where exactly we have oscillations.

**Remarks 3.2 (Solving $(\mathrm{P}_h)$).** (a) The formulae for the Newton-Raphson method for $(\mathrm{P}_h)$ read as (3.5) where $DW$ and $D^2W$ substitutes $DW^{**}$ and $D^2W^{**}$, respectively. This, eventually, corresponds to neglecting the positive parts in the respective formula; $(\cdot)_+$ is replaced by $(\cdot)$.

(b) Our numerical experience strongly suggests that the Newton-Raphson scheme is *not* at all an appropriate numerical algorithm for the computation of discrete solutions of $(\mathrm{P}_h)$. It seems unavoidable to involve energy control, e.g., within some line search algorithm. We found a natural simplified example in 1D where the scheme computed rather a local maximiser of $E|_{\mathscr{A}_h}$ than a local minimiser [7, Figure 7.3] (see [10] for Matlab programs).

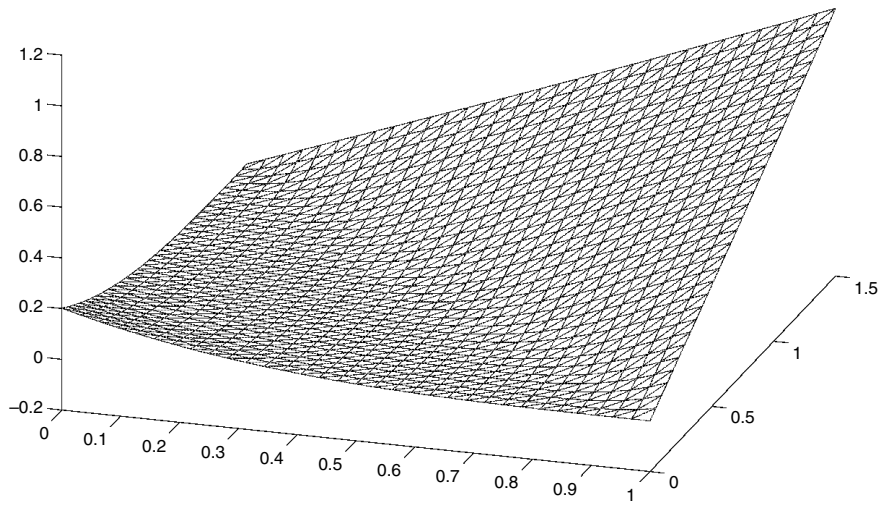


**Fig. 7.** Deformation of $\Omega$ in problem (RP) on a uniform $32 \times 32$ grid with 2048 elements

(c) The numerical solution of ($P_h$) causes, in general, nightmares. We refer to [7, Section 9] for theoretical evidence for cluster of local minimisers around discrete solutions of ($P_h$) in a related 1D example. Typically, any descent method eventually is trapped near a local minimiser. The probability to find the correct discrete solution in practise is very very small.

(d) It should be emphasised that the main advantage and motivation for the numerical treatment of relaxed formulations is that oscillations on a microscopic scale disappear. As a consequence for the model example in this paper, the numerical computation of ($RP_h$) is much cheaper and easier compared to that of ($P_h$). In particular, adaptive algorithms and nested iteration work well for ($RP_h$), but fail for ($P_h$).

(e) The geometry is chosen such that (uniform) meshes are not aligned with the antidiagonal $\Gamma = \mathscr{M} \cap \mathscr{R}$. Parallel to which we expect the layers of a lamination microstructure. Since those layers cannot be resolved on the scale of the mesh-size $h = \sqrt{13}/128 = 0.02817$, we observe the larger microstructure of Figure 4 on a scale $H = 4/(3\sqrt{13})3 = 0.1233$ (if we assume that there are 3/2 layers in Figure 4). Then, $H = h^\alpha$ for $\alpha = 0.586 \approx 2/3$; the latter is suggested by the theoretical investigations in [7, 20, 19] (with $p = 2$ for the growth near the wells).

The generalised solution $u$ and the stress $\sigma$ are known form Theorem 2.1 and hence the errors $||u - u_h||_{L^2(\Omega)}$, $|u - u_h|_{W^{1,4}(\Omega)}$, and $||\sigma - \sigma_h||_{L^{4/3}(\Omega)}$ can be computed. Figure 8 shows various errors for a sequence of uniform meshes. The six curves represent the errors for ($RP_h$) and ($P_h$). The outcome is summarised in the following comments.

**Remarks 3.3 (Discussion on experimental convergence from Figure 8).** (a) The numerical results for ($P_h$) show no convergence. This is theoretically expected for

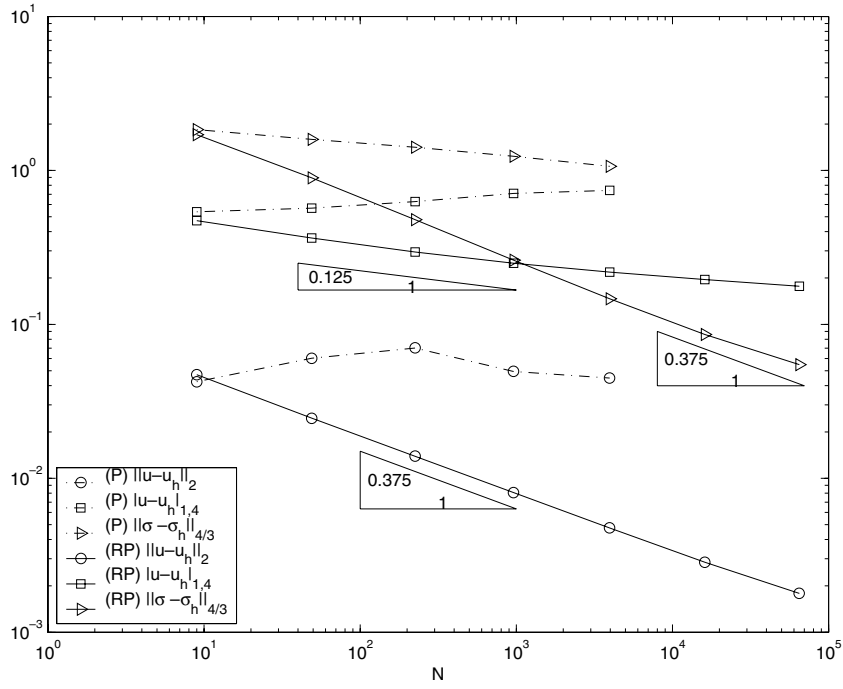


**Fig. 8.** The error in different norms on uniform meshes

the gradients as $|u - u_h|_{W^{1,4}(\Omega)} = O(1)$ but possibly disappointing for $||u - u_h||_{L^2(\Omega)}$. Looking at Figure 4 which shows oscillations of an amplitude of size $H \approx 0.1233$, this explains the large $L^2$ error even for a very fine mesh. The stress error $||\sigma - \sigma_h||_{4/3}$ for $(P_h)$ seems to converge at a very small convergence rate. This behaviour underlines well the overall theoretical observation that the stress field in $(P_h)$ is indeed a macroscopic quantity [6].

(b) The poor convergence rates for $(P_h)$ observed in (a) might be a consequence of (i) a poor numerical approximation $u_h$ or (ii) a coarse mesh even for a $32 \times 32$ grid resolution. Arguments for conjecture (i) include our difficulties reported in Remarks 3.2(a)–(c) as well as the poor resolution of volume fraction or stress fields in Figure 6. A counter argument is the reasonable microstructure on the expected length scale $H$ which, clearly, supports conjecture (ii). Indeed, the mesh seems to be still too coarse to allow a fine resolution with the correct asymptotic behaviour. At least, the microstructure of Figure 4 is affected by boundary conditions and appears very coarse. Hence we cannot really expect to be in an asymptotic range $h \to 0$ and $H \to 0$.

(c) The convergence rates in $(RP_h)$ for $||u - u_h||_2$ and $||\sigma - \sigma_h||_{4/3}$ coincide in agreement with the theoretical prediction of Theorem 3.1.c. From there and with standard interpolation error estimates we would expect

$$||u-u_h||_{L^2(\Omega)} \propto ||\sigma-\sigma_h||_{L^{4/3}(\Omega)} \propto |u-u_h|_{W^{1,4}(\Omega)}$$
$$\propto h^{\alpha} \quad \text{for } u \in W^{1+\alpha,4}(\Omega).$$

The regularity of $u$ is limited to $\alpha = 1/4$ and hence the (lower bound of the) convergence rate $h^{1/4}$ might be expected. Instead, we observe the better convergence rate $h^{3/4}$.

(d) There is no guaranteed convergence rate for the strain error $|u-u_h|_{W^{1,4}(\Omega)} = O(1)$ for ($\mathrm{RP}_h$). In the benchmark example we observe

$$|u-u_h|_{W^{1,4}(\Omega)} \propto h^{1/4}.$$

This improvement clearly leads to non-efficiency of conservative, reliable a posteriori error estimates.

(e) The convergence rates in ($\mathrm{RP}_h$) are non-optimal according to the uniform meshes which do not resolve the jumps in $Du$ across the interface $\Gamma = \mathscr{M} \cap \mathscr{R}$. Since, in practise, location of the free boundary is unknown, we need automatic tools for adaptive mesh-design which steer the refinement effectively. For this purpose, three algorithms are studied in the sequel.

## 4 A posteriori Error Control and adaptive mesh design

Motivated by a lack of regularity of the generalised solution $u$ and resulting sub-optimal convergence of uniform mesh-refinement, this section is devoted to three mesh-refining algorithms for improved convergence rates. We first present the three refinement indicators and the adaptive algorithm and then prove an a posteriori error estimate for their justification.

### *4.1 The Residual Error Indicator*

The analysis in [16] suggests the estimator

$$\eta_R := \left( \sum_{T \in \mathscr{T}} \eta_T^R \right)^{3/8}, \tag{4.1}$$

where, for each $T \in \mathscr{T}$ of size $h_T$ with edges $\mathscr{E}(T)$, $n_E$ the normal and $h_E$ the length of $E \in \mathscr{E}$,

$$\eta_T^R = h_T^{4/3} \int_T |2(f-u_h)|^{4/3} dx + \int_{(\partial T) \cap \Omega} h_E |J(\sigma_h \cdot n_E)|^{4/3} ds. \tag{4.2}$$

(Recall that $J(\sigma_h \cdot n_E)$ denotes the jump of the piecewise constant stresses $\sigma_h$ across interior element boundaries while $J(\sigma_h \cdot n_E) := 0$ on $\partial\Omega$.)

### 4.2 The ZZ-Error Indicator

Given $\sigma_h := DW^{**}(Du_h)$ we define an averaging estimator

$$\eta_Z := \left( \sum_{T \in \mathscr{T}} \eta_T^Z \right)^{3/4}, \tag{4.3}$$

where, for each $T \in \mathscr{T}$,

$$\eta_T^Z := ||\sigma_h - A\sigma_h||_{L^{4/3}(T)}^{4/3}. \tag{4.4}$$

is based on the averaging operator $A$,

$$A\sigma_h = \sum_{z \in \mathscr{N}} \left( \frac{1}{|\omega_z|} \int_{\omega_z} \sigma_h(y) dy \right) \varphi_z,$$

($\omega_z := \bigcup \{T \in \mathscr{T} : z \in T\}$ denotes the patch with area $|\omega_z|$ of a node $z \in \mathscr{K}$).

### 4.3 The D2-Error Indicator

Given $\sigma_h = DW^{**}(Du_h)$ we define

$$\begin{aligned} \tilde{\eta}_{D2} := & \sum_{T \in \mathscr{T}} h_T^2 ||\mathrm{div}_{\mathscr{T}} \sigma_h + 2(f - u_h)||_{L^{4/3}(T)} ||D^2 u||_{L^4(T)} \\ & + \sum_{E \in \mathscr{E}} h_E^{7/4} ||J(\sigma_h \cdot n_E)||_{L^{4/3}(E)} ||D^2 u||_{L^4(T_E)} \end{aligned} \tag{4.5}.$$

Here, $T_E$ is some element $T_E \in \mathscr{T}$ with $E \subseteq \partial T_E$. In the numerical examples, the term $||D^2 u||_{L^4(T)}$ is approximated by weighted jumps $[\nabla u_h] \cdot n_E$ of the piecewise constant gradients $\nabla u_h$ over neighbouring edges $\cup \mathscr{E}(T)$, i.e.,

$$||D^2 u||_{L^4(T)} \approx \left( \sum_{E \in \mathscr{E}(T)} h_E^{-2} |[\nabla u_h] \cdot n_E|^4 \right)^{1/4}. \tag{4.6}$$

The heuristic (4.6) is adapted from (iii) of page 41 in [8] and verified in some easier model examples by numerical experiments. With this heuristic we define the refinement indicator $\eta_{D2}$, for each element $T \in \mathscr{T}$, by

$$\begin{aligned} \eta_T^{D2} := & ||h_T(\mathrm{div}_{\mathscr{T}} \sigma_h + 2(f - u_h))||_{L^{4/3}(T)} \\ & + \left( \sum_{E \in \mathscr{E}(T)} h_E ||J(\sigma_h \cdot n_E)||_{L^{4/3}(E)}^{4/3} \right)^{3/4} \left( \sum_{E \in \mathscr{E}(T)} h_E^{-1} |[\nabla u_h] \cdot n_E|^4 \right)^{1/4}. \end{aligned} \tag{4.7}$$

The following algorithm generates a sequence of refining triangulations with respect to the refinement indicators $\eta_T$ from $\eta_T^R$, $\eta_T^Z$, and $\eta_T^{D2}$.

**Algorithm 4.1 (Adaptive Algorithm).**

(1) *Start with a coarse initial mesh* $\mathscr{T}_{h_0}$, *set* $k = 0$.

(2) *Solve the discrete problem* $u_{h_k}$ *on the mesh* $\mathscr{T}_{h_k}$.

(3) *Compute* $\eta_T$ *for each* $T$ *in* $\mathscr{T}_{h_k}$.

(4) *Compute the upper error bound* $(\sum_{T\in T_{h_k}} \eta_T)^{3/8}$ *and decide to stop* (*then terminate computation*) *or to refine* (*then go to* (5)).

(5) *Mark* $T \in \mathscr{T}_{h_k}$ *for red-refinement provided*

$$\eta_T \geq 1/2 \max_{K\in\mathscr{T}_{h_k}} \eta_K.$$

(6) *Refine further triangles to avoid hanging nodes and thereby create a new mesh* $\mathscr{T}_{h_{k+1}}$ *by red-green-blue refinement. Update* $k$ *to* $k+1$ *and go to* (2).

The three error estimators satisfy the following error estimates.

**Theorem 4.2.** *Let* $u$ *and* $u_h$ *solve (RP) and* (RP$_h$) *with* $\sigma := DW^{**}(Du)$ *and* $\sigma_h := DW^{**}(Du_h)$, *respectively. Then there hold the following a posteriori error estimates.*

(a) $||\sigma - \sigma_h||^{4/3}_{L^{4/3}(\Omega)} + ||u - u_h||^2_{L^2(\Omega)} \leq c_1\eta_R + h.o.t.$

(b) $||\sigma - \sigma_h||^{4/3}_{L^{4/3}(\Omega)} + ||u - u_h||^2_{L^2(\Omega)} \leq c_2\eta_Z + h.o.t.$

(c) *If* $u \in W^{2,4}(\Omega)$ *then* $||\sigma - \sigma_h||^{4/3}_{L^{4/3}(\Omega)} + ||u - u_h||^2_{L^2(\Omega)} \leq c_3\tilde{\eta}_{D2} + h.o.t.$

*The constants* $c_1$, $c_2$, $c_3$ *depend on* $E^{**}(u) + E^{**}(u_h)$ *and the shape of the elements in* $\mathscr{T}$.

**Remark 4.1.** Notice carefully that the error terms on the left-hand side in (a)–(c) are raised in full power 4/3 (resp. 2) while this is not the case for the terms on the right-hand side.

**Remark 4.2.** Details on red-green-blue refinement may be found in [30].

*Sketch of the proof.* Except from proper treatment of $u_D - u_{D,h} \neq 0$ on $\partial\Omega$, the proof of the estimate for the residual error estimate (a) is contained in [16]. We therefore give a sketch of the proof with focus on the new aspects. The point of departure is an elementary estimate for the function $\Sigma := DW^{**} : \mathbb{R}^2 \to \mathbb{R}^2$ which satisfies [30]

$$|\Sigma(A) - \Sigma(B)|^2 \leq 8(\xi(A) + \xi(B) + 2)(\Sigma(A) - \Sigma(B)) \cdot (A - B) \tag{4.8}$$

for all $A, B \in \mathbb{R}^2$ and $\xi : \mathbb{R}^2 \to \mathbb{R}, A \mapsto (|A|^2 - 1)_+$. Let $A = Du$ and $B = Du_h$, raise the resulting inequality to the power 2/3 and integrate over $\Omega$ to obtain

$$||\sigma - \sigma_h||^{4/3}_{L^{4/3}(\Omega)} \leq 4 \int_\Omega (\xi(Du) + \xi(Du_h) + 2)^{2/3}((\sigma - \sigma_h) \cdot D(u - u_h))^{2/3} dx.$$

Hölder's inequality with respect to exponents 3 and 3/2 shows, after raising the result to the power 3/2,

$$||\sigma - \sigma_h||^2_{L^{4/3}(\Omega)} \leq 8||\xi(Du) + \xi(Du_h) + 2||_{L^2(\Omega)} \int_\Omega (\sigma - \sigma_h) \cdot D(u - u_h) dx. \quad (4.9)$$

(Notice carefully that $(\sigma - \sigma_h) \cdot D(u - u_h)$ is non-negative (owing to (4.8)) and so the integral over $\Omega$ equals its $L^1$-norm where it came from.)

For any $v_h \in \mathscr{A}_h$ we have $u_h - v_h = 0$ on $\Gamma_D$ and hence $u_h - v_h \in \mathscr{S}^1_D(\mathscr{T})$ is a linear combination of $(\varphi_z : z \in \mathscr{K})$. The discrete Euler-Lagrange equations of (3.3) therefore lead to

$$\int_\Omega \sigma_h \cdot D(u_h - v_h) dx + 2 \int_\Omega (u_h - f)(u_h - v_h) dx = 0.$$

The continuous version of (2.6) reads

$$\int_\Omega \sigma \cdot D(u_h - v_h) dx + 2 \int_\Omega (u - f)(u_h - v_h) dx = 0.$$

The combination of the two identities shows

$$\int_\Omega (\sigma - \sigma_h) \cdot D(u_h - v_h) dx = \int_\Omega (\sigma - \sigma_h) \cdot D(u_h - v_h) dx + 2 \int_\Omega (u - v_h)(u_h - v_h) dx.$$

This can be re-arranged to

$$\begin{aligned} &\int_\Omega (\sigma - \sigma_h) \cdot D(u - u_h) dx + ||u - u_h||^2_{L^2(\Omega)} \\ &\quad = \int_\Omega (\sigma - \sigma_h) \cdot D(u - v_h) dx + ||u - v_h||^2_{L^2(\Omega)} + ||u_h - v_h||^2_{L^2(\Omega)}. \end{aligned} \quad (4.10)$$

We remark that the combination of (4.9)–(4.10), namely

$$\begin{aligned} &c_h^{-1}||\sigma - \sigma_h||^{4/3}_{L^{4/3}(\Omega)} + ||u - u_h||^2_{L^2(\Omega)} \\ &\quad \leq \int_\Omega (\sigma - \sigma_h) \cdot D(u - v_h) dx + ||u - v_h||^2_{L^2(\Omega)} + ||u_h - v_h||^2_{L^2(\Omega)} =: \text{RHS}, \end{aligned} \quad (4.11)$$

is the basis of a proof of Theorem 3.1.c, where $v_h = Iu$ and $c_h^{-1} := 8||\xi(Du) + \xi(Du_h) + 2||_{L^2(\Omega)}$. For an a posteriori error estimation, we employ the Euler-Lagrange equations (2.6). Given any function $w \in W^{1,4}(\Omega)$ with $w = u_D - u_{D,h}$ on $\partial\Omega$, there holds

$$\int_\Omega \sigma \cdot D(u - u_h - w)\, dx + 2 \int_\Omega (u - f)(u - u_h - w)\, dx = 0.$$

Subtract this from the upper bound RHS of (4.11) to see

$$\begin{aligned} \text{RHS} = &\int_\Omega (\sigma - \sigma_h) \cdot D(w - v_h + u_h)\, dx - 2 \int_\Omega (u - f)(u - u_h - w)\, dx \\ &- \int_\Omega \sigma_h \cdot D(u - u_h - w) dx + ||u - v_h||^2_{L^2(\Omega)} + ||u_h - v_h||^2_{L^2(\Omega)}. \end{aligned} \tag{4.12}$$

The choice $v_h = u_h$ and the identity

$$\begin{aligned} -2 \int_\Omega (u - f)(u - u_h - w)\, dx = &-2 \int_\Omega (u_h - f)(u - u_h - w)\, dx \\ &+ 2 \int_\Omega (u - u_h) w\, dx - ||u - u_h||^2_{L^2(\Omega)} \end{aligned}$$

lead in (4.12) to

$$\begin{aligned} \text{RHS} = &\int_\Omega (\sigma - \sigma_h) \cdot Dw\, dx + 2 \int_\Omega (u - u_h) w\, dx \\ &- 2 \int_\Omega (u_h - f)(u - u_h - w)\, dx - \int_\Omega \sigma_h \cdot D(u - u_h - w)\, dx. \end{aligned}$$

Let us abbreviate the last two terms with the functional by

$$\text{Res}(v) := 2 \int_\Omega (f - u_h)\, dx - \int_\Omega \sigma_h \cdot Dv\, dx.$$

Then, with Hölder's and Young's inequality ($ab \le a^p/p + b^q/q$), we have

$$\begin{aligned} \text{RHS} &= ||\sigma - \sigma_h||_{L^{4/3}(\Omega)} |w|_{W^{1,4}(\Omega)} + 2||u - u_h||_{L^2(\Omega)} ||w||_{L^2(\Omega)} + \text{Res}(u - u_h - w) \\ &\le \frac{3}{4} (c_h^{-3/4} ||\sigma - \sigma_h||_{L^{4/3}(\Omega)})^{4/3} + \frac{1}{4} |w|^4_{W^{1,4}(\Omega)} c_h^3 + \frac{1}{2} ||u - u_h||^2_{L^2(\Omega)} + ||w||^2_{L^2(\Omega)}. \end{aligned}$$

This and (4.11) verify our first new result

$$\begin{aligned} c_h^{-1}||\sigma-\sigma_h||_{L^{4/3}(\Omega)}^{4/3}+2||u-u_h||_{L^2(\Omega)}^2 \\ \leq c_h^3|w|_{W^{1,4}(\Omega)}^4+4||w||_{L^2(\Omega)}^2+4\ \mathrm{Res}(u-u_h-w). \end{aligned} \tag{4.13}$$

The terms with $w$ can be minimised with respect to $w=u_D-u_{D,h}$ on $\partial\Omega$. Given an element $T\in\mathscr{T}$ with $T\cap\partial\Omega=\emptyset$ we define $w|_T\equiv 0$; else we extend $w:=u_D-Iu_D$ from $(\partial T)\cap(\partial\Omega)$ by zero to $\partial T$. Then we extend $w$ from $\partial T$ to $T$ with midpoint $z$ of the largest interior circle by a convex combination: $w(x)=\lambda w(y)$ for $x=\lambda y+(1-\lambda)z$. Then,

$$\begin{aligned} |\nabla w|_{1,\infty,T} &\lesssim ||w/h_T||_{\infty,\partial T}+||\partial_{\mathscr{E}}w/\partial s||_{\infty,\partial T}\lesssim h_T||\partial_{\mathscr{E}}^2u_D/\partial s^2||_{\infty,\Gamma_D}, \\ ||w||_{\infty,T} &\lesssim ||w||_{\infty,\partial T}\lesssim h_T^2||\partial_{\mathscr{E}}^2u_D/\partial s^2||_{\infty,\Gamma_D}. \end{aligned}$$

Here and below, $A\lesssim B$ abbreviates $A\leq cB$ with a generic constant $c$ which depends on the shape of the elements but not on their sizes. (Recall that $w$ is zero at the vertices of $\partial T$ and hence $||w||_{\infty,\partial T}\lesssim||\partial_{\mathscr{E}}^2u_D/\partial s^2||_{\infty,\Gamma_D}$ for the edgewise derivative $\partial_{\mathscr{E}}$ etc.) Since only a boundary layer of elements leads to $w\neq 0$, this shows $|w|_{W^{1,4}(\Omega)}^4+||w||_{L^2(\Omega)}=o(h)=h.o.t.$ Notice that $\xi(A)^2\leq W^{**}(A)$ for any $A\in\mathbb{R}^2$. Hence

$$\begin{aligned} c_h &\leq 24(4+\int_\Omega W^{**}(Du)dx+\int_\Omega W^{**}(Du_h)dx) \\ &\leq 24(4+E^{**}(u)+E^{**}(u_h))\leq 480 \end{aligned}$$

for $E^{**}(u_h)\leq E^{**}(u)+0.89$, i.e., for sufficiently small mesh sizes. (Recall that we have convergence of the energy according to a density argument and even convergence rates in terms of $h$ by convexity).

It therefore remains to estimate $\mathrm{Res}(u-u_h-w)$. One major property of the functional Res is

$$\mathrm{Res}(v_h)=0\quad\text{for all } v_h\in\mathscr{S}_0^1(\mathscr{T}), \tag{4.14}$$

a direct consequence of the discrete characterisation in (3.3). Set $v:=u-u_h-w\in W_0^{1,4}(\Omega)$. The first estimation of $\mathrm{Res}(v-v_h)$ essentially follows [16] in an elementwise integration by parts, a trace estimate, a Clément-type approximation, and, finally, Cauchy estimates to deduce

$$\mathrm{Res}(v)\lesssim|u-w|_{W^{1,4}(\Omega)}\eta_R\leq(c+\text{h.o.t.})\eta_R. \tag{4.15}$$

This proves (a); more details (with $w=0$) may be found in [16].

As it was known to the experts before, the edge contributions dominate in $\eta_R$ [18]. Following [11, 13] we consider an approximation operator $J: W_0^{1,p}(\Omega)\to\mathscr{S}_0^1(\mathscr{T})$ with the following first-order approximation and $W^{1,p}$-stability property

$$||h_{\mathscr{T}}^{-1}(v-Jv)||_{L^p(\Omega)} + |v-Jv|_{W^{1,p}(\Omega)} \lesssim |v|_{W^{1,p}(\Omega)}, \tag{4.16}$$

plus an extra local orthogonality property,

$$\int_\Omega (v-Jv)g\,dx \lesssim ||h^2\nabla g||_{L^q(\Omega)}|v|_{W^{1,p}(\Omega)} \tag{4.17}$$

for all $v \in W_0^{1,p}(\Omega)$ and $g \in W^{1,p}(\Omega)$. We follow [6] and consider an arbitrary $\tau_h \in \mathscr{S}^1(\mathscr{T})^2$ and integrate $\int_\Omega \tau_h \cdot D(v-Jv)dx$ by parts. Then,

$$\begin{aligned}\mathrm{Res}(v-Jv) &= 2\int_\Omega (f-u_h)(v-Jv)dx - \int_\Omega \tau_h \cdot D(v-Jv)dx \\ &\quad + \int_\Omega (\tau_h-\sigma_h)\cdot D(v-Jv)dx \\ &= \int_\Omega (2f-2u_h+\mathrm{div}\ \tau_h)(v-Jv)dx + \int_\Omega (\tau_h-\sigma_h)\cdot D(v-Jv)dx.\end{aligned}$$

With (4.16)–(4.17) we deduce

$$\begin{aligned}\mathrm{Res}(v-Jv) \lesssim \Big(&||h_{\mathscr{T}}^2 Df||_{L^{4/3}(\Omega)} + ||h_{\mathscr{T}}^2 Du_h||_{L^{4/3}(\Omega)} \\ &+ ||h_{\mathscr{T}}\mathrm{div}\tau_h||_{L^{4/3}(\Omega)} + ||\sigma_h-\tau_h||_{L^{4/3}(\Omega)}\Big)|v|_{W^{1,4}(\Omega)}.\end{aligned} \tag{4.18}$$

An inverse estimate (employed separately for each element) yields

$$||h_{\mathscr{T}}\mathrm{div}_{\mathscr{T}}\tau_h||_{L^{4/3}(\Omega)} = ||h_{\mathscr{T}}\mathrm{div}(\sigma_h-\tau_h)||_{L^{4/3}(\Omega)} \lesssim ||\sigma_h-\tau_h||_{L^{4/3}(\Omega)}.$$

($\mathrm{div}_{\mathscr{T}}\tau_h$ is the piecewise divergence, hence $\mathrm{div}_{\mathscr{T}}\sigma_h = 0$.) Since $Du_h$ is bounded in $L^4$, the first two terms in (4.18) are $O(h^2)$. Hence we deduce

$$\mathrm{Res}(v-Jv) \lesssim |u-u_h-w|_{W^{1,4}(\Omega)}\Big(\mathrm{h.o.t.} + ||\sigma_h-\tau_h||_{L^{4/3}(\Omega)}\Big). \tag{4.19}$$

This and (4.13) prove (b).

The verification of (c) follows the proof of (a) to the estimation of $\mathrm{Res}(v-v_h)$ for $v = u-u_h-w$ and $v_h = Iu-u_h$. An elementwise integration by parts (as in the proof of (a)) leads to

$$\mathrm{Res}(v-v_h) = \int_\Omega (\mathrm{div}_{\mathscr{T}}\sigma_h + (f-u_h))(v-v_h)dx + \int_{\bigcup\mathscr{E}} J(\sigma_h\cdot n_{\mathscr{E}})(v-v_h)dx. \tag{4.20}$$

With Cauchy inequalities, this leads to

$$\begin{aligned}\mathrm{Res}(v-v_h) \le \sum_{T\in\mathscr{T}} ||\mathrm{div}\sigma_h + (f-u_h)||_{L^{4/3}(T)} ||u - Iu - w||_{L^4(T)} \\ + \sum_{E\in\mathscr{E}_\Omega} ||J(\sigma_h\cdot n_E)||_{L^{4/3}(E)} ||u-Iu-w||_{L^4(E)}.\end{aligned} \tag{4.21}$$

Notice that $u - Iu - w = 0$ on $\partial\Omega$ and $w = 0$ on $(\bigcup \mathscr{E}) \cap \Omega$ by the above choice of $w \in H^1(\Omega)$; $\mathscr{E}_\Omega$ denotes the interior edges in $\mathscr{E}$. Recall that $||w||_{L^4(\Omega)} \lesssim O(h_T^2) h_T^{1/2}$. A trace inequality from [12], namely

$$||u-Iu-w||^4_{L^4(E)} \lesssim h_T^{-1} ||u-Iu-w||^4_{L^4(T)} + h_T^3 ||D(u-Iu-w)||^4_{L^4(T)}, \tag{4.22}$$

leads to

$$\begin{aligned}\mathrm{Res}(v-v_h) &\lesssim \sum_{T\in\mathscr{T}} ||\mathrm{div}_{\mathscr{T}}\sigma_h + (f-u_h)||_{L^{4/3}(T)} ||u-Iu-w||_{L^4(T)} \\ &\quad + \sum_{E\in\mathscr{E}} ||J(\sigma_h\cdot n_E)||_{L^{4/3}(E)} \Big( h_T^{-1} ||u-Iu||^4_{L^4(T)} + h_T^3 ||D(u-Iu)||^4_{L^4(T)} \Big)^{1/4} \\ &\le \sum_{T\in\mathscr{T}} h_T^2 ||\mathrm{div}_{\mathscr{T}}\sigma_h + (f-u_h)||_{L^{4/3}(T)} \Big( ||D^2 u||_{L^4(T)} + o(1) \Big) \\ &\quad + \sum_{E\in\mathscr{E}} ||J(\sigma_h\cdot n_E)||_{L^{4/3}(E)} \Big( h_T^{-1} h_T^8 ||D^2 u||^4_{L^4(T)} + h_E^7 ||D^2 u||^4_{L^4(E)} \Big)^{1/4} \\ &\lesssim \sum_{T\in\mathscr{T}} h_T^2 ||\mathrm{div}_{\mathscr{T}}\sigma_h + (f-u_h)||_{L^{4/3}(T)} \Big( ||D^2 u||_{L^4(T)} + o(1) \Big) \\ &\quad + \sum_{E\in\mathscr{E}} h_E^{7/4} ||J(\sigma_h\cdot n_E)||_{L^{4/3}(E)} ||D^2 u||_{L^4(T_E)}. \qquad \square\end{aligned}$$

## 5 Numerical Experiments

This section is devoted to answer several questions empirically for the benchmark proposed in the previous sections.

### *5.1 Resolution of Free-Boundary*

Although there is no free boundary formulation in the strict sense (of free boundary problems), the interface $\Gamma = \mathscr{M} \cap \mathscr{R}$ between the regions with and without enforced microstructures in unknown a priori and gives, at least in our

benchmark example, rise to discontinuous gradients. For the uniform mesh-refinements of Figure 4 (for (P)) and Figure 7 (for (RP)), the deformation near that straight line is not clearly resolved as for $Iu$ of Figure 3. The three adaptive mesh-refining algorithms, namely the $\eta_R$, $\eta_Z$, and $\eta_{D2}$ indicated versions of Algorithm 4.1, generate sequences $\mathscr{T}_0, \mathscr{T}_1, \ldots$ of meshes. The mesh $\mathscr{T}_{15}$ is displayed in its deformed configuration in Figure 9–11 with $N = 2462$, $N = 2485$, and $N = 1188$ degrees of freedom for ($\mathrm{RP}_h$).

Figure 9–11 illustrate the generalised solution and resolve the discontinuity along $\Gamma$ quite clearly. This is achieved by local refinements along $\Gamma$.

### *5.2 Approximation of Young Measures*

The formation of microstructure is parallel to $\Gamma$ and this is not aligned with the original mesh $\mathscr{T}_0$. Discrete approximations of Young measure based on the discrete displacements from ($\mathrm{RP}_h$) can be computed from (2.9). The corresponding figures are very similar to Figure 5 and hence not displayed. Our interpretation is that the adaptive refinement along $\Gamma$ resolves the Young measure more appropriate than uniform refinements. Similar remarks apply to stress fields as well and, therefore, we do not show corresponding figures.

### *5.3 Stress Improvements*

The error $||\sigma - \sigma_h||_{4/3}$ can be computed and Figures 12–15 show $||\sigma - \sigma_h||_{4/3}$ versus the number of degrees of freedom. For uniform meshes and $\eta_R$, $\eta_Z$, or $\eta_{D2}$

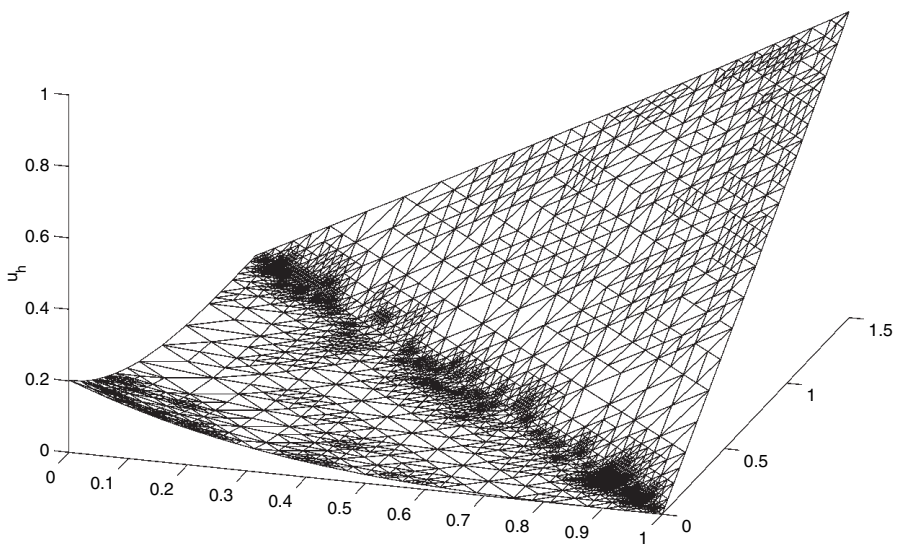


**Fig. 9.** Mesh $\mathscr{T}_{15}$ refined with the indicator $\eta_R(N = 2462)$

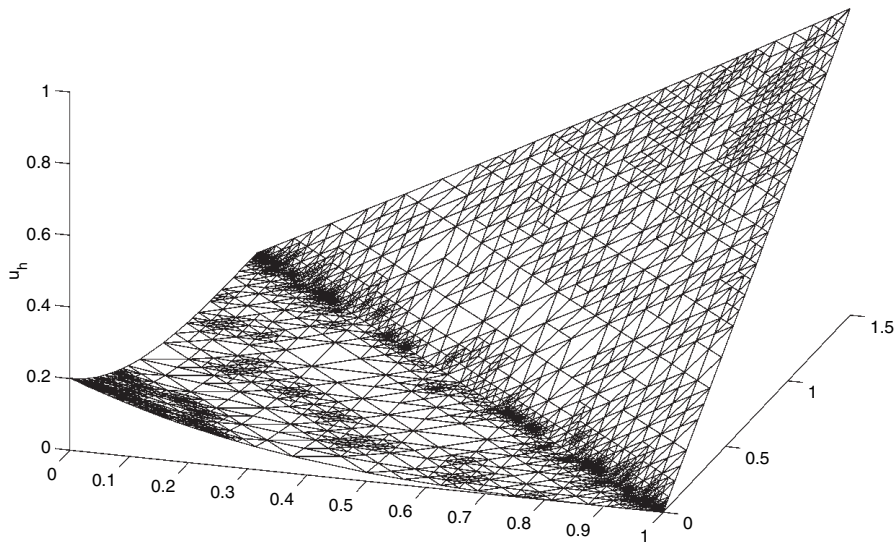


**Fig. 10.** Mesh $\mathscr{T}_{15}$ refined with the indicator $\eta_Z(N = 2485)$

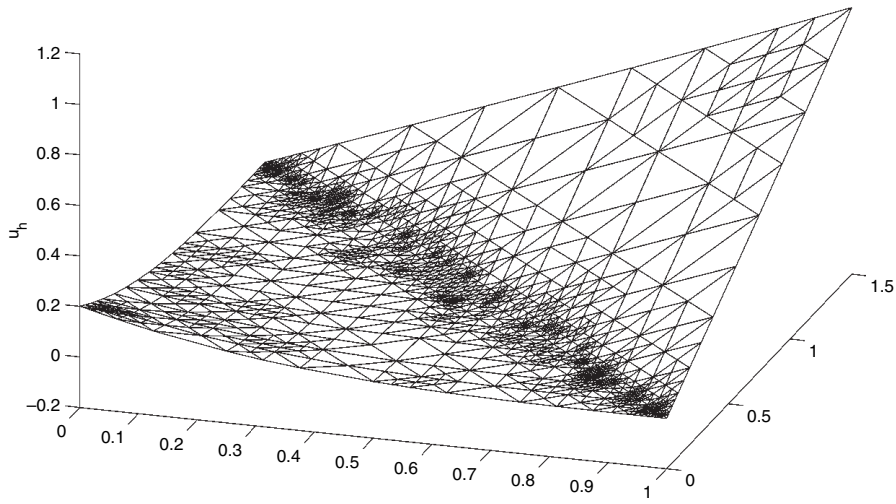


**Fig. 11.** Mesh $\mathscr{T}_{15}$ refined with the indicator $\eta_{D2}(N = 1188)$

adapted meshes we further computed the three estimators $\eta_R$, $\eta_Z$, $\eta_{D2}$ as in (1.8) and (1.11). This yields sequences of meshes in each of Figure 12, 13, and 14. A uniform mesh results in an experimental convergence rate 3/8 for the error $||\sigma - \sigma_h||_{4/3}$ and the estimators $\eta_Z$ and $\eta_{D2}$ while we see half of that convergence rate for the reliable $\eta_R$. The adaptive meshes show an improved convergence rate 1 for $||\sigma - \sigma_h||_{4/3}$, $\eta_Z$, and $\eta_{D2}$ while $\eta_R$ converges with rate 3/8.

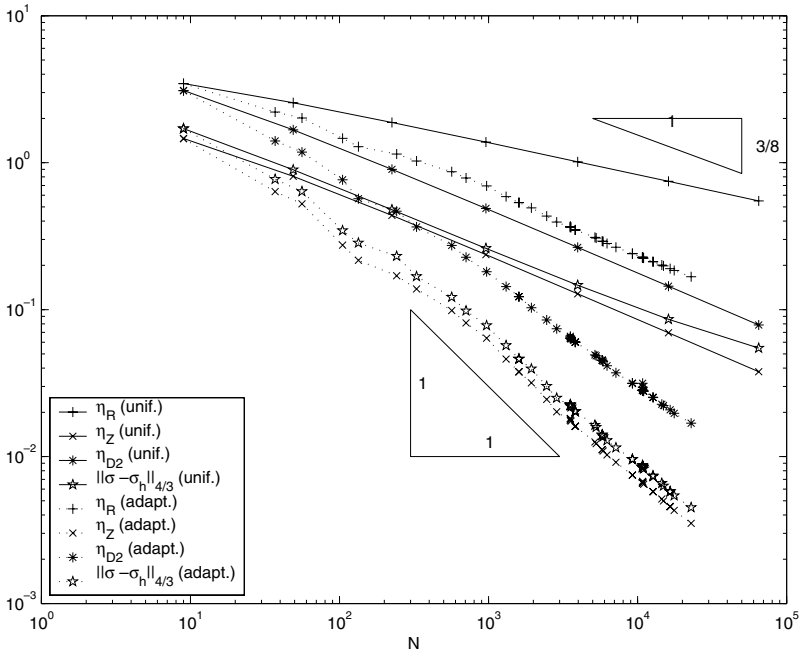


**Fig. 12.** The error estimates $\eta_R$, $\eta_Z$, $\eta_{D2}$ compared with the stress error $||\sigma - \sigma_h||_{4/3}$ for uniform and $\eta_R$ adapted meshes

### *5.4 Effective Mesh-Refinement*

Figure 12 and 13 give empirical evidence that all three adaptive algorithms yield optimal stress convergence. To answer the question which method is the best, the stress error is displayed in Figure 14 for uniform $\eta_R$, $\eta_Z$, $\eta_{D2}$ adapted meshes. The convergence rates are optimal as explained, but, in absolute terms, $\eta_R$ and $\eta_{D2}$ give comparable accuracy slightly less sharp than $\eta_Z$. Our overall interpretation is that any reasonable adaptive algorithm improves the situation.

### *5.5 Accurate Error Estimation*

It is obvious from the previous discussion on Figures 12–14 that $\eta_R$ (although reliable) is too conservative. The reliable ignorance of $||D(u - u_h)||_4$ in (1.9) is not efficient. The progressive estimation with $||h_{\mathcal{T}} D^2 u||_4$ requires the heuristic evaluation through $||h_{\mathcal{E}}^{-1/2}[\nabla u_h] \cdot n_{\mathcal{E}}||_{L^2(\bigcup_{\mathcal{E}})}$. This step lacks a theoretical justification and so we address this question empirically. From the reliable and effective performance of $\eta_{D2}$ in all our experiments we can agree with [8] that this replacement leads in our benchmark to reasonable numerical results. The overestimation by a factor could be improved by a different scaling, i.e., by a substitution of $\eta_{D2}$ by $0.1\eta_{D2}$, as suggested in [8].

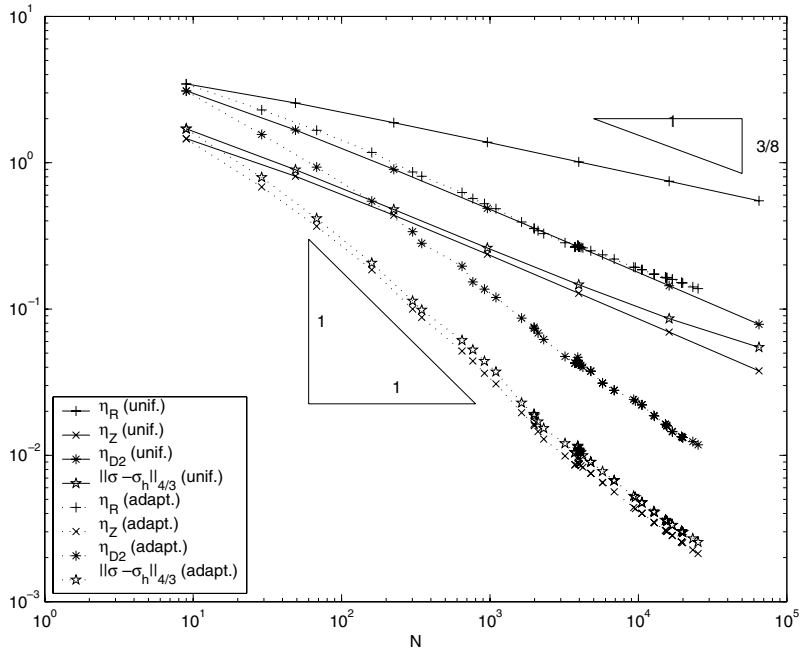


**Fig. 13.** The error estimates $\eta_R$, $\eta_Z$, $\eta_{D2}$ compared with the stress error $||\sigma - \sigma_h||_{4/3}$ for uniform and $\eta_Z$ adapted meshes

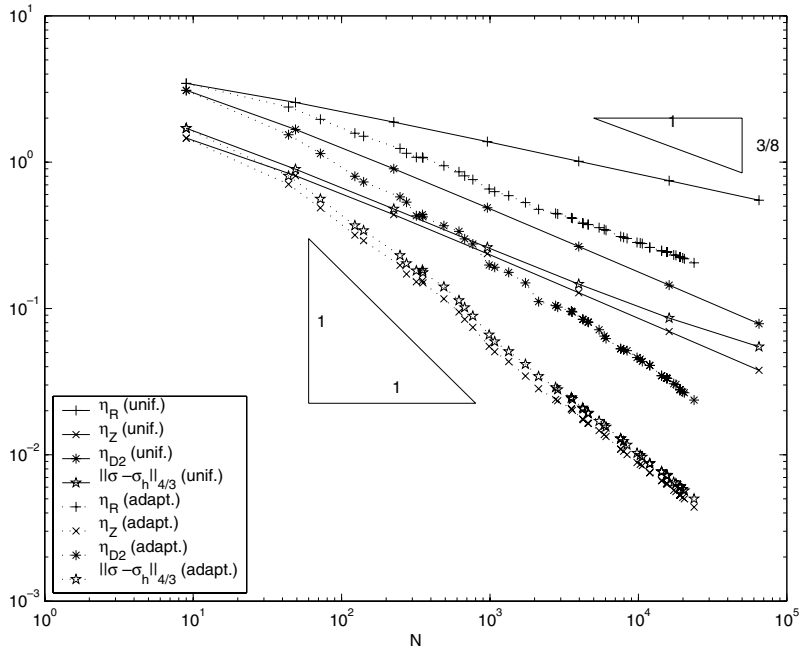


**Fig. 14.** The error estimates $\eta_R$, $\eta_Z$, $\eta_{D2}$ compared with the stress error $||\sigma - \sigma_h||_{4/3}$ for uniform and $\eta_{D2}$ adapted meshes

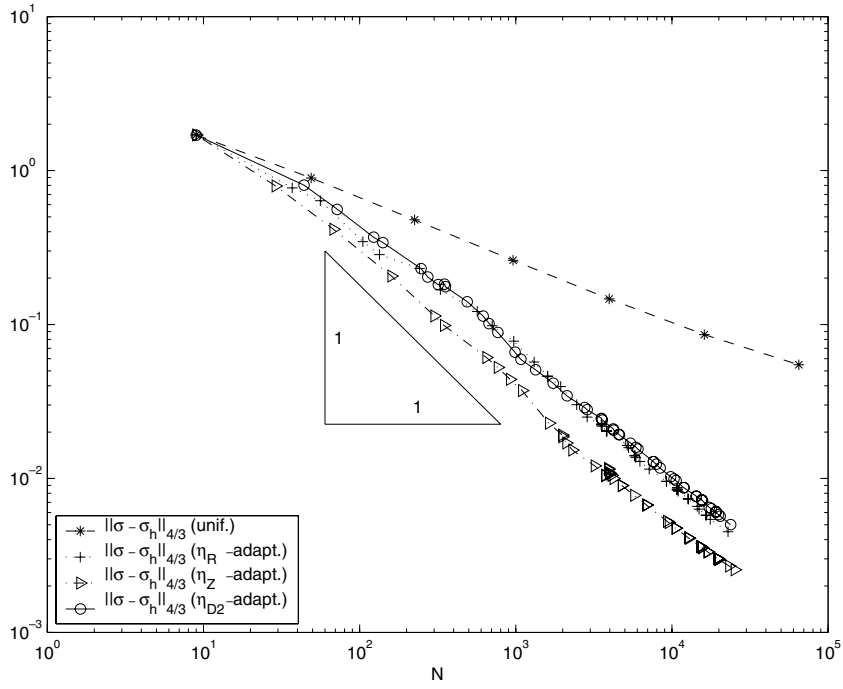


**Fig. 15.** The stress error $||\sigma - \sigma_h||_{4/3}$ for uniform and $\eta_R$, $\eta_Z$, $\eta_{D2}$ adapted meshes

The most striking aspect, however, is the amazing accuracy of the averaging estimator, $\eta_Z \approx ||\sigma - \sigma_h||_{4/3}$. This is in agreement with numerical experiments on uniformly convex experiments in [11, 13, 14].

### *5.6 Adaptive Mesh Refinements for ($P_h$)*

In contrast to a general warning in [10] (i.e. 'Do not use adaptive algorithms for non-convex minimisation problems!') our corresponding numerical experience (not displayed) indicates that, partly, the adapted meshes show a slightly improved stress error. For finer meshes, however, numerical difficulties (indicated in Remarks 3.2 b–d) prevent us from giving a clear evidence. Nevertheless, at the moment, adaptive algorithms for ($P_h$) lack *any* theoretical justification.

## Acknowledgements

The research was supported by the Max Planck Institute in the Sciences of Leipzig, Germany, by the German Research Foundation through the DFG-Schwerpunktprogramm Multi-Scale Problems (SPP 1095), and by the Isaac Newton Institute for Mathematical Sciences of Cambridge, UK, also through EPSRC (GR N09176/01).

## References


[1] Alberty, J., Carstensen, C., Funken, S. A.: Remarks around 50 lines of Matlab: Finite element implementation. Numerical Algorithms *20*, 117–137 (1999).

[2] Ball, J. M.: A version of the fundamental theorem for young measures. In Partial differential equations and continuum models of phase transitions, Lecture Notes in Physics *344*, 207–215 (1989).

[3] Ball, J. M.: Singularities and computation of minimisers for variational problems. In Proceedings of Foundations of Computational Mathematics Conference, Oxford: Cambridge University Press 1999.

[4] Ball, J. M., James, R. D.: Fine phase mixtures as minimisers of energy. Arch. Rational Mech. Analysis *100*, 13–52 (1987).

[5] Ball, J. M., James, R. D.: Proposed experimental tests of the theory of fine microstructure and the two–well problem. Phil. Trans. R. Soc. Lond. A. *338*, 389–450 (1992).

[6] Ball, J. M., Kirchheim, B., Kristensen, J.: Regularity of quasiconvex envelopes. Calc. Var. *11*, 333–359 (2000).

[7] Bartels, S., Prohl, A.: Multiscale resolution in the computation of crystalline microstructure. Numer. Math. (2003) accepted for publication.

[8] Becker, R., Rannacher, R.: An optimal control approach to a posteriori error estimation in finite element methods. Acta Numerica 1–102 (2001).

[9] Bethuel, F., Huisken, G., Müller, S., Steffen, K.: Variational models for microstructure and phase transitions. In: Calculus of variations and geometric evolution problems. Springer LNM *1713*, 85–210 (1999).

[10] Carstensen, C.: Numerical analysis of microstructure. Theory and numerics of differential equations, Durham 2000, Univeritext, p 59–126, Berlin Heidelberg: Springer 2001.

[11] Carstensen, C., Bartels, S.: Each averaging technique yields reliable a posteriori error control in FEM on unstructured grids part I: Low order conforming, nonconforming, and mixed FEM. Math. Comp. *71*, 945–969 (2002).

[12] Carstensen, C., Funken, S. A.: Constants in Clément-interpolation error and residual based a posteriori estimates in finite element methods. East-West-Journal of Numerical Analysis *8, 3*, 153–175 (2000).

[13] Carstensen, C., Funken, S. A.: Averaging technique for FE - a posteriori error control in elasticity. Part I: Conforming FEM. Comput. Methods Appl. Mech. Engrg. *190*, 2483–2498 (2001). Part II: $\lambda$-independent estimates. Comput. Methods Appl. Mech. Engrg. *190*, 4663–4675 (2001). Part III: Locking-free nonconforming FEM. Comput. Methods Appl. Mech. Engrg. *191*, 8–10, 861–877 (2001).

[14] Carstensen, C., Klose, R.: Guaranteed a posteriori finite element error control for the p-Laplace problem. SIAM J. Sci. Comput. (2003), In Press.

[15] Carstensen, C., Müller, S.: Local stress regularity in scalar non-convex variational problems. SIAM J. Math. Anal. *34*, 495–509 (2001).

[16] Carstensen, C., Plecháč, P.: Numerical solution of the scalar double-well problem allowing microstructure. Math. Comp. *66*, 997–1026 (1997).

[17] Carstensen, C., Plecháč, P.: Numerical analysis of compatible phase transitions in elastic solids. SIAM J. Numer. Anal. *37, 6*, 2061–2081 (2000).

[18] Carstensen, C., Verfürth, R.: Edge residuals dominate a posteriori error estimates for low order finite element methods. SIAM J. Numer. Anal. *36, 5*, 1571–1587 (1999).

[19] Chipot, M.: Elements of nonlinear analysis. Birkhäuser (2000).

[20] Chipot, M., Müller, S.: Sharp energy estimates for finite element approximation of non-convex problems. In: IUTAM Symposium on variations of domains and free-boundary problems in solid mechanics, p 317–325, Kluwer 1999.

[21] Chipot, M., Evans, L. C.: Linearisation at infinity and Lipschitz estimates for certain problems in the calculus of variations. Proc. R. Soc. Edinburgh *102A*, 291–303 (1986).

[22] Dacorogna, B.: Direct methods in the calculus of variations. Applied Mathematical Sciences *78* (1989).

[23] Friesecke, G.: A necessary and sufficient condition for non-attainment and formation of microstructure almost everywhere in scalar variational problems. Proc. R. Soc. Edin. *124A*, 437–471 (1994).

[24] Kristensen, J.: On the non-locality of quasiconvexity. Annales de l'Institut Henri Poincaré (C) Analyse non linéaire *16, 1*, 1–13 (1999).

[25] Luskin, M.: On the computation of crystalline microstructure. Acta Numerica *5*, 191–257 (1996).

[26] Nicolaides, R. A., Walkington N.J.: Strong convergence of numerical solutions to degenerate variational problems. Math. Comp. *64*, 117–127 (1995).
[27] Pedregal, P.: Parametrised measures and variational principles. Birkhäuser (1997).
[28] Roubíček, T.: Relaxation in optimization theory and variational calculus. Series in nonlinear analysis and application, *4* (1997).
[29] Tartar, L.: Private communication (1999).
[30] Verfürth, R.: A review of a posteriori error estimation and adaptive mesh-refinement techniques. Wiley-Teubner (1996).

C. Carstensen
Institute for Applied Mathematics and
Numerical Analysis,
Vienna University of Technology,
Wiedner Hauptstraße 8-10,
A-1040 Vienna
Austria
e-mail: Carsten.Carstensen@tuwien. ac.at

K. Jochimsen
Mathematisches Seminar,
Christian-Albrechts-Universität zu Kiel,
Ludewig-Meyn-Str. 4,
D-24098 Kiel,
Germany

Verleger: Springer-Verlag KG, Sachsenplatz 4–6, A-1201 Wien. – Herausgeber: Prof. Dr. Wolfgang Hackbusch, Max-Planck-Institut für Mathematik in den Naturwissenschaften, Inselstraße 22–26, D-04103 Leipzig – Satz und Umbruch: Scientific Publishing Services (P) Ltd., Madras; Offsetdruck: Manz Crossmedia. 1051 Wien. – Verlagsort: Wien. – Herstellungsort: Wien. – Printed in Austria.